Thermodynamic estimation of liquidus, solidus, Ae_3 temperatures, and phase compositions for low alloy multicomponent steels

In an attempt to develop improved models for the prediction of microstructures in steel weld deposits, established thermodynamic procedures have been used to estimate the liquidus, solidus, and Ae_3 transformation temperatures for multicomponent steels, together with partitioning coefficients and other parameters. The method has been tested against a large amount of published data and there is found to be good agreement between experiment and theory.

MST/975

A. A. B. Sugden
H. K. D. H. Bhadeshia

 Manuscript received 25 August 1988; in final form 14 February 1989. *The authors are in the Department of Materials Science and Metallurgy, University of Cambridge.*

Introduction

The majority of steel weld deposits solidify under highly non-equilibrium cooling conditions. A consequence of this is the chemical segregation of substitutional alloying elements during solidification, a segregation that persists as the weld cools to ambient temperature. Solidification induced segregation of interstitials is usually not a problem because of the ease with which they can diffuse and homogenise during cooling. The presence of substitutional element segregation can greatly influence the subsequent transformation of austenite into ferrite with reaction kinetics in general being accelerated in the solute depleted regions. The formation of ferrite in these regions causes a redistribution of carbon into the remaining austenite, the hardenability of which is therefore increased. It has been demonstrated[1] that such effects can have a major influence on the development of microstructure and any method for alloy design must take them into proper consideration.

Weld metals typically solidify as δ-ferrite and subsequently transform to austenite γ and then to ferrite α. To obtain a general model for the prediction of the properties of a weld metal, it will be necessary to be able to predict the chemical segregation behaviour during solidification. For low alloy C–Mn steel weld deposits solidifying as δ-ferrite, solute enriched prior δ-boundaries will finish up approximately within the centre of the austenite grains. The effect of the segregation will be to increase the temperature at which allotriomorphic ferrite initially transforms and to increase the temperature range over which α forms. Hence, the ultimate volume fraction for a given set of cooling conditions will increase.[2] Conversely, for solidification as austenite, since regions in the proximity of the austenite boundaries would be solute enriched, nucleation of α would be expected to be more difficult.[1] To predict weld metal segregation quantitatively will necessarily require a knowledge of the solidification temperature, solidification range, level of partitioning in the melt, and partition coefficients for the carbon and solute elements in the steel. The present work is an attempt at modelling the high temperature region of the phase diagram for multicomponent steels, using the general thermodynamic procedures developed by Kirkaldy and co-workers.[3,4] To verify the consistency of the present calculations and of the thermodynamic data used, calculations were also attempted for the α/γ equilibria, where the amount of experimental data available as a verification of theory is much greater.

Method of analysis

One of the most important factors which must be considered in thermodynamic modelling of the Fe–C–X multicomponent system is that it ceases to retain the characteristics of infinite dilution for concentrations above $\sim$0·2 wt-%C (Refs. 5, 6). In the analysis of Kirkaldy and Baganis,[3] which is used in the present work, this problem is circumvented by determining the temperature deviation of a particular phase boundary from the corresponding boundary in the binary Fe–C system. The change in carbon concentration at a phase boundary, due to the addition of substitutional alloying elements, is given by summing the effects due to each individual element.

In the following description, iron is designated as 0, carbon as 1, and the alloying elements Si, Mn, Ni, Cr, Mo, Cu, V, Nb, Co, W as $i(=2\text{–}n)$. The mole fractions in each phase are designated as $X_i(i=0\text{–}n)$. A general temperature coordinate on a phase boundary in the pure Fe–C system is designated T_o. The temperature deviation from T_o due to this addition of substitutional elements ΔT is calculated for the required range of T_o, so that the phase boundary $T\{\text{Fe–C–X}_i\}$ may be found. This procedure follows the classical 'depression of the freezing point' relationship derived by Van't Hoff (*see* Ref. 5). In multicomponent alloys, these temperature changes resulting from individual alloy additions are additive as long as solute–solute interactions are negligible. The interactions between elements in solution are represented by empirical coefficients known as the Wagner interaction parameters and the above assumption of additive ΔT values is the same as saying that the interaction between elements i and k, $\varepsilon_{ik}(i \neq k,\ i \text{ and } k > 1) = 0$. In fact, this is not strictly correct[7] and silicon, especially, can interact with other solute elements.[8] However, Kirkaldy and co-workers[3,4] found that this assumption is valid as long as the total alloying element content is less than $\sim$6 wt-% and the silicon content is <1 wt-%.

To calculate the temperature deviation at a phase boundary ΔT, Kirkaldy and Baganis[3] started with the relationship for the equality of the chemical potentials in

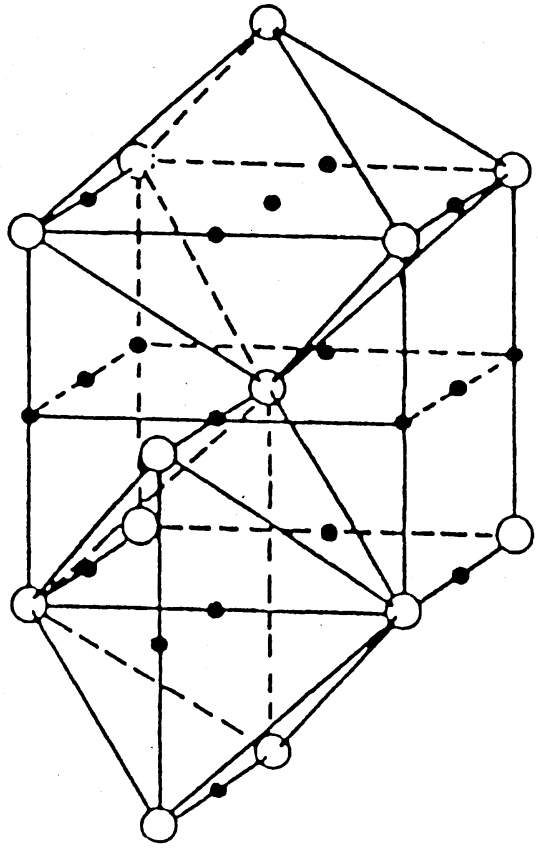

1 Location of the octahedral interstices (●) in bcc crystal (After Ref. 16)

the two phases which are in equilibrium. For example, for the austenite and liquid/liquid phase boundary for iron

$$X_0^\gamma \gamma_0^\gamma = X_0^L \gamma_0^L \exp\left(\frac{\Delta^\circ G_0^{\gamma \to L}}{RT}\right) \quad \ldots\ldots\ldots \quad (1)$$

where $X_0 = 1 - \Sigma_{i=1}^{n} X_i$ is the mole fraction of iron, γ_0 is the activity coefficient for the iron, and the superscripts γ and L denote the austenite and liquid phases, respectively. In this equation, $\Delta^\circ G^{\gamma \to L} = {}^\circ G_L - {}^\circ G_\gamma$ or, more generally, the difference between the Gibbs free energies of the pure higher and lower temperature phases, T is the phase boundary temperature and R is the universal gas constant.

Similarly for carbon($n = 1$) or component i

$$X_i^\gamma \gamma_i^\gamma = X_i^L \gamma_i^L \exp\left(\frac{\Delta^\circ G_i^{\gamma \to L}}{RT}\right) \quad \ldots\ldots\ldots \quad (2)$$

The Wagner–Taylor expansions for the activity coefficients[9] were then substituted into equations (1) and (2). Eventually, this gave the temperature deviation in the form

$$\Delta T = RT_o^2 \sum_{i=2}^{n} A_i X_i^L \quad \ldots\ldots\ldots \quad (3)$$

where X_i^L is the mole fraction of component i and where

$$A_i = \frac{A_i^0 - [1 + X_1^L(1 - X_1^L)(\varepsilon_{1i}^L - \varepsilon_{11}^\gamma A_1^0 A_i^0)] \exp B}{[X_1^L \Delta^\circ H_1 A_1^0 + (1 - X_1^L)\Delta^\circ H_0] \exp B}$$

for which

$$B = \left\{\frac{\Delta^\circ G_0}{RT_o^2} - \frac{(X^L)^2}{2}[\varepsilon_{11}^L - \varepsilon_{11}^\gamma (A_1^0)^2]\right\}$$

and

$$A_n^0 = \frac{\exp[(\Delta^\circ G_n/RT_o) + \varepsilon_{1n}^L X_1^L]}{1 + \varepsilon_{1n}^\gamma X_1^L \exp(\Delta^\circ G_1/RT_o)}$$

where $n = 1$ or i (Ref. 4), and $\Delta^\circ H_0$ and $\Delta^\circ H_1$ are the standard molar enthalpy changes corresponding to $\Delta^\circ G_0$ and $\Delta^\circ G_1$, respectively.

This was the relationship used for the determination of the Fe–C–X_i multicomponent equilibrium phase diagram. The solute elements for which the program has been written are those that might commonly be found in low alloy steels (Mn, Si, Ni, Cr, Mo, and Cu) although, if the relevant free energy changes per unit of solute dissolving $\Delta^\circ G$ and the interaction parameters ε are known, ΔT can in principle be calculated for any alloy.

Prediction of Ae_3 temperature

The overall intention of this and other current research is to be able to predict the mechanical properties of multipass welds. This requires a detailed knowledge of the thermal history of the weld and necessarily of the transformation temperatures of the steels. In welding, the Ae_3 temperature has a considerable influence on, *inter alia*, the relative volume fractions of the phases present in the as welded microstructure and the size of the reaustenitised region in multipass welds. Therefore, as an initial step, a program was written to allow the Ae_3 temperature to be predicted, using the method described above. A series of modifications was incorporated into it as follows.

1. The program had been used for Mn, Si, Ni, Cr, Mo, and Cu additions.[3] In addition, the elements for Nb, Co, V, and W were included, using further data given by Kirkaldy *et al.*[4]

2. The Ae_3 values for T_o were formulated into a subroutine using accurate values derived from equations from Bhadeshia and Edmonds[10] giving values of T_o down to 200°C. Extrapolating the Ae_3 in this manner would be potentially very useful, allowing, for example, growth rate kinetics to be calculated at temperatures well below the eutectoid temperature.[11]

3. Although data were provided[12] for values for the standard Gibbs free energy change accompanying the α/γ transformation in pure iron $\Delta^\circ G_0^{\alpha \to \gamma}$, since a longterm aim was to extrapolate the Ae_3 to lower temperatures, the data from Kaufman *et al.*,[13] which give values down to 0 K and which are known to be reliable over an entire temperature range of interest,[14] were used. The function $\Delta^\circ G_0^{\alpha \to \gamma}$ was represented by curve fitting values from Table 3 of Kaufman *et al.*[13] and later corrected values for $\Delta^\circ G_0^{\alpha \to \gamma}(T > 1183\ \text{K})$ from Kaufman and Bernstein.[15]

4. Values for $\Delta^\circ H_0^{\alpha \to \gamma}$ were obtained from work carried out by Kaufman *et al.*[13]

In applying equation (3) to the calculation of the Ae_3, Kirkaldy and Baganis[3] had taken ε_{11}^α as zero. They argued that the error introduced is negligible, since the interaction parameter is multiplied only by the very low concentration of carbon in ferrite. This assumption can be assessed quantitatively. Figure 1 shows the carbon sublattice in a crystal of α-Fe. The bcc unit cell contains two iron atoms and six carbon sites. (This ignores tetrahedral sites, but the probability of their occupation is rather low.) The maximum solubility of carbon in δ-Fe is 0·09 wt-% = 0·417 at.-%. Therefore, there are (99·6/0·417) = 239 iron atoms for every carbon atom, or there is one carbon atom for every 119 unit cells, so that, even at saturation, the probability of two carbon atoms even being in the same unit cell is only 0·004. Thus, the

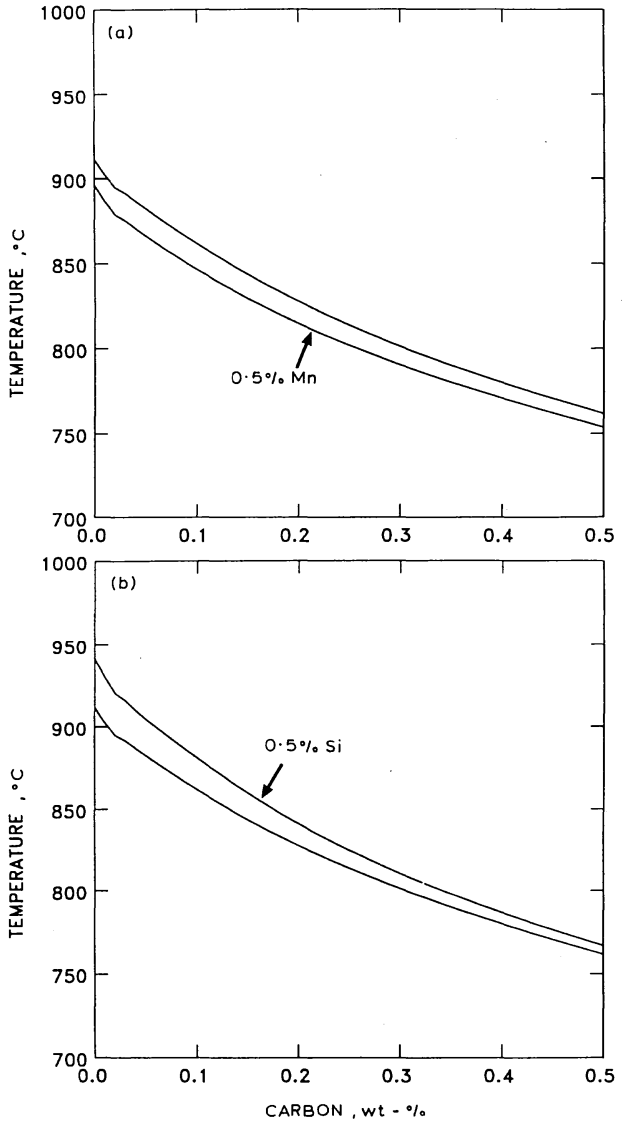

2 Vertical sections of Fe–C–X phase diagrams, showing effect on Ae_3 temperature of adding 0·5 wt-% of *a* manganese and *b* silicon to binary Fe–C

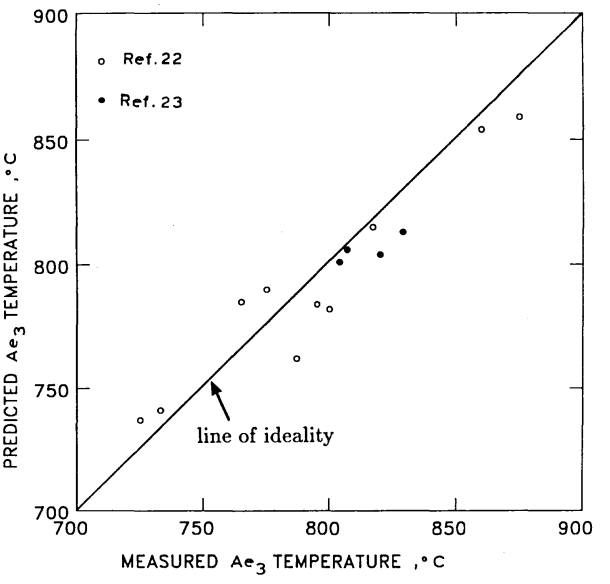

3 Comparison of predicted and measured values for Ae_3 temperature for various steels

assumption made by Kirkaldy and Baganis seems justified and was adopted.

Since all the thermodynamic functions used were dependent on temperature, ΔT cannot be obtained from a single application of equation (3), but must be deduced iteratively. For this purpose, a loop was included in the program. Initially, T was set as T_0 and a trial value of ΔT was calculated. Then, the program was rerun with $T = (T + \Delta T)$. This procedure was repeated until the value of T changed by less than 0·1 K in successive iterations (typically five times). Results for all the alloying elements were determined and verified for correspondence with data from Fe–X binary phase diagrams compiled by Kubaschewski;[17] overall agreement was excellent. However, discrepancies were observed with the Fe–Mn, and Fe–Nb systems, and these are discussed below.

Fe–Mn

As Kirkaldy and Baganis[3] also found, a systematic discrepancy was observed between experimental and calculated values for the Fe–Mn system, attributable to errors in $\Delta^\circ G^{\alpha\rightarrow\gamma}_{Mn}$. Instead, data were used from Gilmour *et al.*,[18] who calculated $\Delta^\circ G^{\alpha\rightarrow\gamma}_{Mn}$ between 700 and 850°C using experimental results on the Fe–C–Mn system. In their work, $\Delta^\circ G^{\alpha\rightarrow\gamma}_{Mn}$ was calculated as a function of temperature from a knowledge of the activity and molar concentrations of manganese in austenite and ferrite at equilibrium to give*

$$\Delta^\circ G^{\alpha\rightarrow\gamma}_{Mn} = 25{\cdot}57T - 32\,640 \quad \ldots\ldots\ldots \quad (4)$$

Fe–Nb

A large deviation from the α/γ phase boundary was found because of an error in $\Delta^\circ G^{\alpha\rightarrow\gamma}_{Nb}$. Kirkaldy *et al.*[4] give

$$\Delta^\circ G^{\alpha\rightarrow\gamma}_{Nb} = 60{\cdot}0 - 5{\cdot}4\times10^{-3}T \quad \ldots\ldots\ldots \quad (5)$$

In fact, this value was due to a mistake in the original source[19] in applying the equation due to Andrews[20] relating the excess molar Gibbs free energy to the solute concentration in the two phases. Recalculating with respect to niobium (rather than pure iron) gives

$$\Delta^\circ G^{\alpha\rightarrow\gamma}_{Nb} = -RT\ln\left|\frac{X^{\gamma}_{Nb}}{X^{\alpha}_{Nb}}\right| \quad \ldots\ldots\ldots \quad (6)$$

At 1262 K, $X^{\gamma}_{Nb} = 6{\cdot}0\times10^{-3}$ and $X^{\alpha}_{Nb} = 1{\cdot}1\times10^{-2}$ (Ref. 21). At 1493 K, $X^{\gamma}_{Nb} = 1{\cdot}2\times10^{-2}$ and $X^{\alpha}_{Nb} = 1{\cdot}6\times10^{-2}$ (Ref. 19). Therefore, $\Delta^\circ G^{\alpha\rightarrow\gamma}_{Nb}$ may be expressed as

$$\Delta^\circ G^{\alpha\rightarrow\gamma}_{Nb} = 2{\cdot}1596\times10^{4} - 12{\cdot}073T \quad \ldots\ldots\ldots \quad (7)$$

With this recalculation, the discrepancy disappeared.

Figures 2*a* and *b* show two examples from the Ae_3 program and illustrate well the effect on the Ae_3 temperature of adding 0·5 wt-%Mn, when the austenite phase field expands, and 0·5 wt-%Si, when the Ae_3 temperature is increased as the austenite phase field contracts.

Experimental data for high purity Fe–C–X alloys, together with data for a broad range of steels, were used to check the accuracy of the program. The conditions imposed were that $\Sigma_{i=2}^{n} X_i \leqslant 6$ wt-%, as Kirkaldy and Baganis[3] advised, so that solute–solute interactions could realistically be assumed to be negligible, and that the silicon content was restricted to less than 1 wt-% because the Wagner interaction coefficients $\varepsilon^{\alpha}_{ii}$ and $\varepsilon^{\gamma}_{ii}$ for silicon are very large compared with those for other alloying elements. Figure 3 uses data from Aaronson and Domain[22] and Swinden and Woodhead,[23] who established Ae_3 tempera-

* $\Delta^\circ G$ is in J mol^{-1} and T is in K unless stated otherwise.

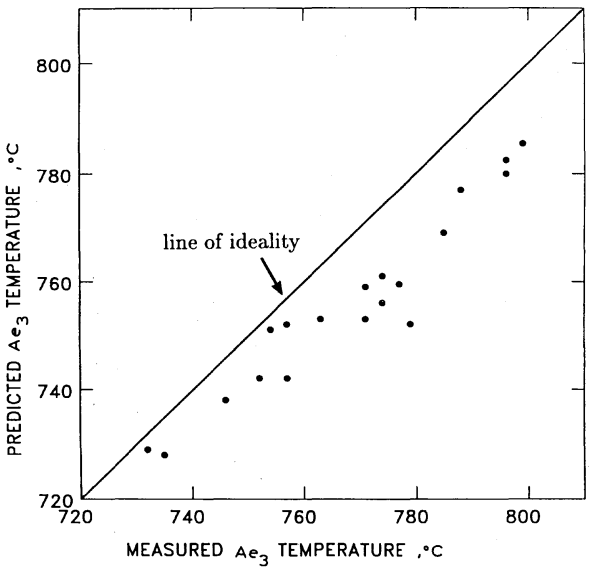

4 Experimental and calculated values for Ae_3 temperature, using experimental data from Ref. 24

tures for a series of experimental steels containing Mn, Si, Ni, Cr, Mo, Cu, and Co. It can be seen that the general agreement between predictions and measurements is very good, the standard error being less than ± 10 K. Data were also taken from Grange[24] consisting of an analysis of 19 medium carbon low alloy steels of commercial purity. Grange identified the Ae_3 temperature as the temperature at which the last trace of ferrite transformed to austenite on prolonged isothermal heating. This work,[24] as with dilatometry on heating, would be liable to yield higher than true equilibrium values. This is in agreement with the results obtained in Figure 4, the mean apparent overshoot of the experimental results obtained being slightly less than 10 K.

Prediction of peritectic region

LIQUIDUS TEMPERATURE

Over recent years it has become apparent[25,26] that the mode of solidification is a determining factor in the subsequent development of the weld metal microstructure. However, to attempt to model the mode of solidification would require a knowledge of the steel's solidification behaviour. Although equation (3) had been applied widely to the prediction of the Ae_3 temperature, the accuracy of the equation at predicting the liquidus and other peritectic temperatures of low alloy multicomponent steels does not seem to have been verified. Kirkaldy and Baganis[3] did compute the peritectic part of the phase diagram for several ternary alloys, but their calculations do not seem to have been compared against experimental data.

Most of the data required were already found in Kirkaldy *et al.*[4]* However, several phase boundaries on the binary phase diagram were not included in that analysis; these were the ferrite and austenite solidi, and the $\delta/\delta+\gamma$ line. Also, the equation given in Kirkaldy *et al.*[4] for T_o for the austenite liquidus as a function of carbon due to Benz and Elliott[27] did not seem to match published ASM data[28] and a new curve was calculated. From the Fe–C equilibrium phase diagram the lines were calculated, respectively, to be

$$T_o^{\delta \rightarrow \delta+L} = 1809 - 201{\cdot}3(\text{wt-\%C}) - 2949(\text{wt-\%C}) \quad . \quad (8a)$$

$$T_o^{\gamma \rightarrow \gamma+L} = 1793 - 146{\cdot}7(\text{wt-\%C}) - 16{\cdot}74(\text{wt-\%C})^2 \quad . \quad (8b)$$

$$T_o^{\gamma+\delta \rightarrow \delta} = 1666 + 1122(\text{wt-\%C}) \quad . \quad (8c)$$

$$T_o^{\gamma+L \rightarrow L} = 1783 - 164{\cdot}0(\text{wt-\%C}) - 7{\cdot}869(\text{wt-\%C})^2 \quad . \quad (8d)$$

To discover if any data values were suspect, the carbon content X_1^L was set to zero so that dilute binary phase diagrams were generated for each element. In this manner, the value of ΔT for each solute element could be verified. Although general agreement was excellent, a systematic discrepancy was found for the Fe–Mn system, and in the present work $\Delta^\circ G_{Mn}^{\alpha \rightarrow L}$ has been estimated from values for $\Delta^\circ G_{Mn}^{\alpha \rightarrow \delta}$ and $\Delta^\circ G_{Mn}^{\gamma \rightarrow L}$. Kirkaldy *et al.*[4] give

$$\left.\begin{aligned} \Delta^\circ G_{Mn}^{\gamma \rightarrow \delta} &= 2{\cdot}72 \times 10^3 - 1{\cdot}28T \\ \Delta^\circ G_{Mn}^{\gamma \rightarrow L} &= 1{\cdot}20 \times 10^4 - 8{\cdot}50T \end{aligned}\right\} \quad . \quad (9)$$

These two functions are then combined to give

$$\Delta^\circ G_{Mn}^{\alpha \rightarrow L} = \Delta^\circ G_{Mn}^{\delta \rightarrow \gamma} + \Delta^\circ G_{Mn}^{\gamma \rightarrow L}$$
$$= 9{\cdot}25 \times 10^3 - 7{\cdot}22T \quad . \quad (10)$$

As with the Ae_3 program, a temperature loop was included in the program to increase the accuracy of the final result.

To assess the overall accuracy of the program, experimental data were taken from Jernkontoret,[29] in which values for the liquidi, solidi, and solidification ranges of a wide range of steels have been measured by differential thermal analysis at a variety of cooling rates. In addition, newly published experimental data from Howe,[30] giving the liquidus temperatures of a wide range of steels, were used. The compositions of the steels for which $\Sigma_{i=2}^{n} X_i \leqslant 6$ wt-% are given in Table 1. For this analysis, data from Ref. 29 obtained at the lowest cooling rates (0·1 K s^{-1}) were used, since these are expected to be closest to equilibrium. Experimental and calculated values for the liquidus temperatures of the steels given in Table 1 are listed in Table 2 and plotted in Fig. 5. It can be seen that agreement

Table 1 Compositions, of low alloy multicomponent steels analysed, wt-%

Steel no.	C	Si	Mn	Cr	Mo	Ni	Cu	Nb	V
201	0·11	0·12	1·25	0·06	0·07	0·03	0·07	...	...
202	0·12	0·27	1·53	0·02	0·03	0·03	0·05	...	...
203	0·18	0·44	1·26	0·01	0·06	0·02	0·02	0·03	...
204	0·19	0·40	1·42	0·07	0·02	0·13	0·08	...	...
205	0·36	0·27	0·58	0·08	0·02	0·05	0·12	...	...
206	0·69	0·23	0·72	0·02	0·01	0·02	0·03	...	...
207	1·01	0·25	0·46	0·02	0·02	0·03	0·03	...	...
209	0·20	0·25	0·90	0·81	0·06	1·05	0·07	...	0·02
211	0·29	0·21	0·62	1·11	0·21	0·15	0·04	...	0·04
213	0·35	0·24	0·67	0·92	0·19	0·05	0·07	...	0·02
214	0·52	0·22	0·85	1·07	0·07	0·07	0·04	...	0·14
216	1·01	0·23	0·33	1·55	0·01	0·02	0·04	...	0·04
1	0·30	0·10	0·13	0·30	0·024	0·05	...	...	...
2	0·48	0·06	0·04	0·08	0·016	0·015	...	...	...
3	0·66	0·31	0·04	0·04	0·007	0·015	...	...	...
4	0·81	0·41	0·04	0·03	0·012	0·02	...	...	...
5	0·58	0·99	< 0·02	0·03	< 0·02	< 0·02	...	...	...
6	0·89	0·43	< 0·02	0·02	< 0·02	< 0·02	...	...	...
7	1·20	0·53	< 0·02	< 0·02	< 0·02	0·03	...	...	...
8	1·48	0·55	< 0·02	0·02	< 0·02	0·04	...	...	...
25	0·004	0·11	0·14	0·03	...	...	...	...	...
26	0·001	0·32	0·02	0·04	0·005	0·02	...	...	...

Data for steels 201–216 taken from Ref. 29 and for steels 1–26 from Ref. 30.

* The data in Kirkaldy *et al.*[4] contain the following errata:
1. $\Delta^\circ G_{Mn}^{\alpha \rightarrow \gamma} = -26\,650 + 42{\cdot}69T - 0{\cdot}017T^2$ cal mol^{-1}, not $0{\cdot}17T^2$.
2. $\Delta^\circ G_{Mn}^{\gamma \rightarrow \delta} = 430 - 0{\cdot}305T$ cal mol^{-1}, not 650.
3. $\Delta^\circ G_{Mn}^{\alpha \rightarrow \gamma} = 3500 - 2{\cdot}308T$ cal mol^{-1}, not 3100.
4. Table 3 should be headed $\Delta^\circ G_i^{\gamma \rightarrow L}$, not $\Delta G_i^{\alpha \rightarrow L}$.
5. $\Delta^\circ H_1^{\gamma \rightarrow L} = -5360$ cal mol^{-1}, not -5630.
6. $T_o^{\gamma \rightarrow \gamma+\alpha} = 1185 - 150{\cdot}3$ wt-%C $+ 216(0{\cdot}865$ wt-%C$)^{4{\cdot}26}$ K, not 1115.

Equation 1 and, in Appendix 1, equations 2, 14, 17, 18, 21, and 22 also contain typographical errors; the reader is referred to the present text and to Ref. 3. In addition, in Tables 1–3 the standard state superscripts are omitted.

Table 2 Measured and predicted values for liquidus temperatures of 22 low alloy steels

Steel no.	Primary solidification mode	Measured liquidus temperature, °C	Predicted liquidus temperature, °C
201	Ferritic	1515	1523
202	Ferritic	1514	1520
203	Ferritic	1507	1516
204	Ferritic	1506	1514
205	Ferritic	1501	1507
206	Austenitic	1474	1479
207	Austenitic	1459	1458
209	Ferritic	1503	1505
211	Ferritic	1503	1508
213	Ferritic	1495	1504
214	Austenitic	1483	1485
216	Ferritic	1451	1454
1	Ferritic	1505	1516
2	Ferritic	1470	1500
3	Austenitic	1476	1482
4	Austenitic	1464	1470
5	Austenitic	1472	1477
6	Austenitic	1456	1465
7	Austenitic	1437	1441
8	Austenitic	1408	1419
25	Ferritic	1529	1534
26	Ferritic	1530	1532

is excellent and actually better than that achieved for the Ae_3, the slight overestimation for the liquidus being attributable perhaps to the measurements being made under continuous cooling conditions.

SOLIDIFICATION AS PRIMARY AUSTENITE

The small differences in Gibbs free energy between various equilibria in the Fe–C system means that metastable equilibria should also be considered, since metastable phases may be kinetically favoured. Depending upon the composition and cooling conditions, steels may solidify directly as austenite or ferrite and, in general, the close proximity of the liquidus surfaces of these two phases means that metastable formation of one phase may occur when equilibrium data indicate[31,32] that the other phase is the stable one. One particular advantage of using thermochemical calculations is that the $\gamma/\gamma+L$ phase boundary is readily calculable. High cooling rates can obviate nucleation

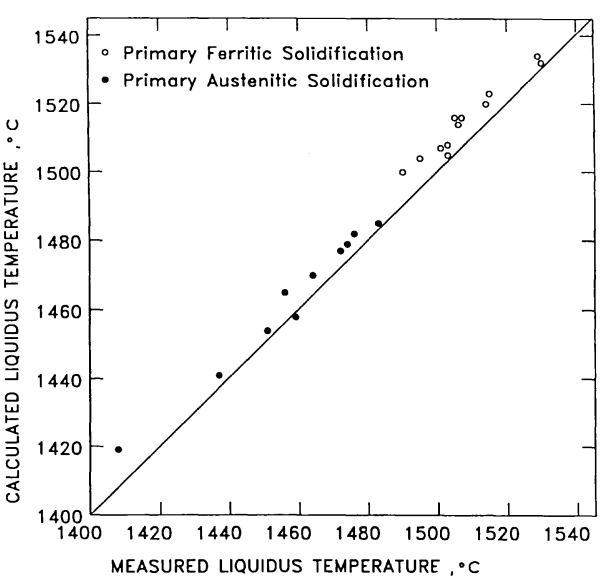

5 Predicted and measured liquidus temperatures for 22 low alloy steels for primary ferrite and primary austenite solidification; data are taken from Refs. 29 and 30

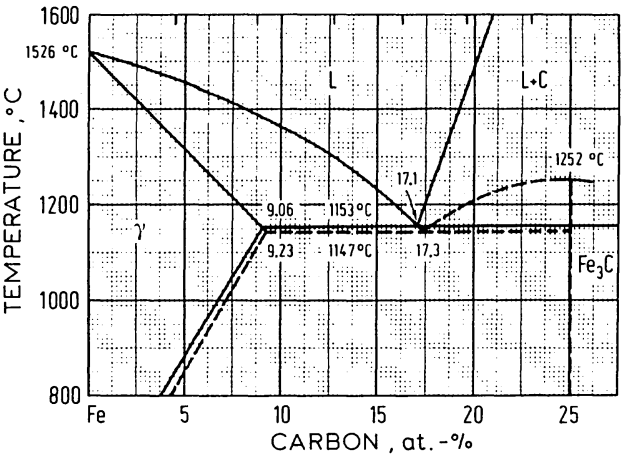

——— stable boundaries
– – – boundaries of austenite–cementite equilibria

6 Fe–C equilibria of austenite with graphite and cementite (After Ref. 17); γ austenite, L liquid phase

of the δ-phase above the peritectic temperature, so that solidification then proceeds according to the austenite–cementite system. Since solute elements have different solubilities and diffusion rates in ferrite and in austenite, segregation is directly influenced by the form of the primary precipitation. Specifically, the diffusion rate of substitutional elements in ferrite is two orders of magnitude greater than in austenite and consequently segregation during a ferritic solidification process is much less than during an austenitic process.[33] This behaviour has profound significance in welding since solidification as austenite will result not only in differences in solute segregation, but also in the distribution of the inclusions in the weld with respect to the phases that subsequently form.

Figure 6 shows the austenite–graphite and austenite–cementite phase diagram, where the stable boundaries are indicated by full lines and the boundaries of the austenite–cementite equilibria by dashed lines. This metastable system has been constructed in the program by extrapolating the austenite solidus and austenite liquidus. It can be seen that the melting point of γ-Fe is only $\sim$10 K lower than the melting point of δ-Fe.

PREDICTION OF SOLIDIFICATION RANGES

Solidification of an alloy with a finite freezing range can allow the formation of an inhomogeneous solid and the amount of eventual segregation may be directly related to the solidification range of the alloy. Therefore, it was crucial to verify the accuracy of the program at predicting the solidus temperatures and solidification ranges of the steels

Table 3 Calculated and measured solidi and solidification ranges for steels analysed

Steel no.	Solidus temperature, °C		Solidification range, °C	
	Measured	Predicted	Measured	Predicted
201	1455	1471	60	52
202	1460	1460	54	60
203	1460	1470	47	46
204	1460	1467	46	47
205	1440	1442	61	65
206	1370	1383	104	96
207	1340	1321	119	137
209	1445	1459	58	46
211	1450	1450	53	58
213	1425	1440	70	64
214	1400	1410	83	75
216	1300	1318	151	136

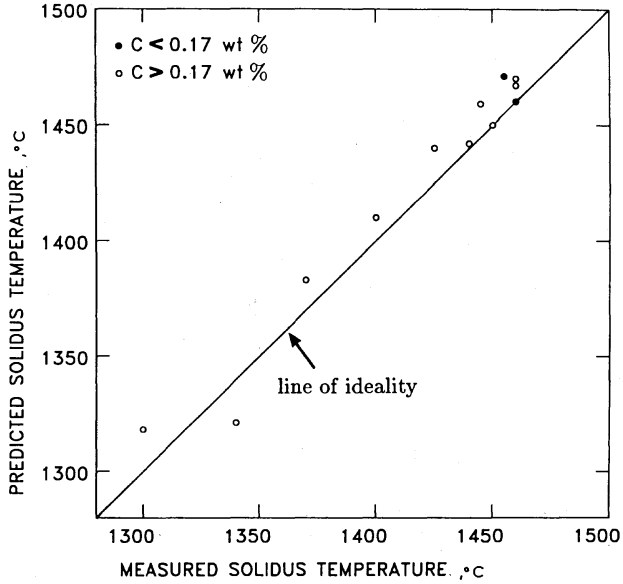

7 Experimental and calculated values for solidus temperature of range of 12 low alloy multicomponent steels; data are from Ref. 29 (0·17 wt-%C corresponds to peritectic point on binary Fe–C equilibrium phase diagram and thus indicates change in solidification mode for alloys)

analysed. For steels 201 and 202, which respectively contain 0·11 and 0·12 wt-%C and which solidify through the peritectic as δ-ferrite, the δ-solidus was estimated, to a first approximation, by extrapolation of the δ-solidus line. For the other steels, it was calculated from the austenite solidus. Table 3 lists measured and predicted values of the solidus temperatures and solidification ranges for the Jernkontoret steels. These data are plotted in Figs. 7 and 8, respectively. As with the liquidus, it can be seen that the thermodynamic algorithm is an excellent predictor of both the solidus temperature and the solidification range of the steels.

Figures 9*a* and *b* show the entire peritectic region drawn using the computer model. The figures show two constant sections through the Fe–C–Mn and Fe–C–Cr phase diagram for 0 and 1·0%Mn and 0 and 2·0%Cr, (wt-%)

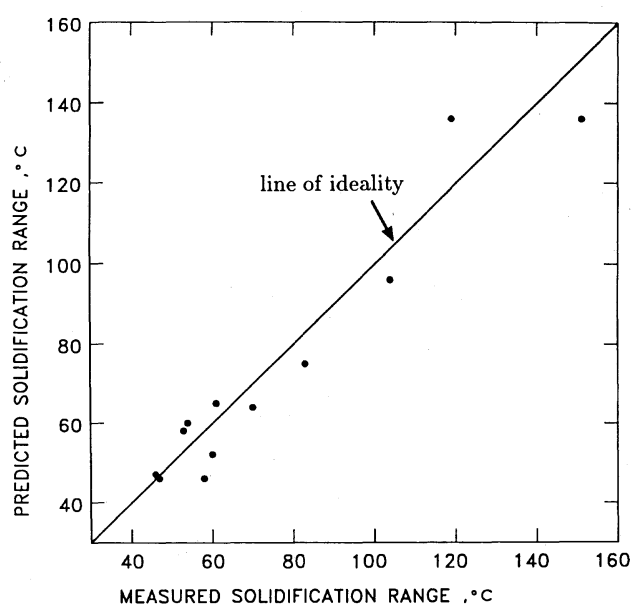

8 Experimental and calculated values for solidification range of 12 low alloy steels given in Table 1

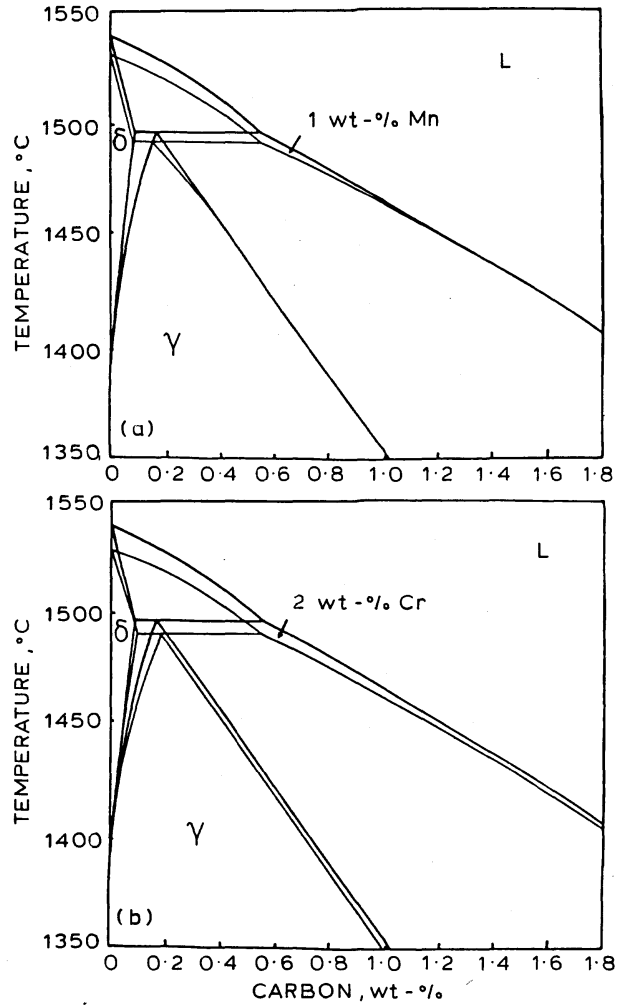

9 Phase diagrams for *a* Fe–C–Mn and *b* Fe–C–Cr; diagrams were constructed using points generated by computer model (it should be noted that, for simplicity, three phase peritectic region has been maintained as straight line)

respectively. Although, the exact composition of the phases in microscopic equilibrium cannot be predicted from a vertical section of the phase diagram, it is possible to do so for trends in compositional change. Depression of the peritectic and Ae_3 temperatures can be seen. Stabilisation of the austenite phase field and a concomitant contraction of the δ-phase field for manganese, and the corresponding expansion of the δ-field and contraction of the austenite field when chromium is present, should also be noted.

Calculation of partition coefficients

The partition coefficient of a solute element is a characteristic value showing the level of microsegregation of an element in an alloy system. To determine the equilibrium partition coefficients of solute elements for multicomponent systems entails time consuming experiments. Therefore, the application of thermodynamic calculations to the determination of partition coefficients is a logical step, particularly since, for a dilute solution containing small amounts of alloying elements, the contribution from the interaction among the elements to the partition coefficient between δ-ferrite or austenite and liquid iron is negligible.[7] Since the cooling rates encountered in welding are fairly high, it can

Table 4 Prediction of liquidus equilibrium partition coefficients

(X_i^δ/X_i^L)		(X_i^γ/X_i^L)	
Measured	Predicted	Measured	Predicted
Ref. 34			
0·90	0·78	0·95	0·77
0·91	0·72	0·50	0·82
0·95	0·84	0·87	0·69
0·83	0·50	0·95	0·62
0·86	0·50	0·60	0·36
0·96	0·77	0·50	0·28
0·95	0·78	...	...
0·94	0·88	...	...
Ref. 35			
0·84	0·78	...	...
0·80	0·72	...	...
0·88	0·84	...	...
0·83	0·50	...	...
0·50	0·50	...	...
Ref. 36			
0·73	0·78	0·78	0·78
0·66	0·72	0·50	0·82
0·95	0·84	0·95	0·69
0·75	0·50	0·75	0·62
0·74	0·50	0·74	0·36
0·70	0·72	0·70	0·90
0·95	0·78	...	...
0·92	0·88	...	...

be assumed that segregation occurring during solidification is not influenced by subsequent diffusion during cooling from the liquidus.[1] By considering the steel at a temperature at which both the ferrite and austenite are in equilibrium, the proportions of these two phases and their composition (i.e. the partition of the alloy elements) can also be calculated. The partition coefficient of a given solute element is determined using the relationship given in equation (3). For example, for the γ–L transformation,

$$X_i = X_i^L A_i \quad \ldots\ldots\ldots\ldots\ldots\ldots \quad (11)$$

where

$$A_i = \frac{\exp\left(\frac{\Delta^\circ G_i}{RT_o} + \varepsilon_{1i}^L X_1^L\right)}{1 + \varepsilon_{1i}^\gamma X_1^L \exp\frac{\Delta^\circ G_i}{RT_o}}$$

Values for the equilibrium partition coefficients of the major alloying elements between δ-Fe and liquid iron (X_i^δ/X_i^L) and between austenite and liquid iron (X_i^γ/X_i^L) have been calculated and are given in Table 4 together with experimental data.

Agreement for solidification as δ-ferrite (Fig. 10*a*) is fair. The reason for the poorer agreement for solidification as austenite in (Fig. 10*b*) is not obvious, although even here equation (11) describes qualitatively the relative effects of the various solute elements. However, in future work, the use of more detailed models[7,36] to describe partitioning in the melt may be necessary.

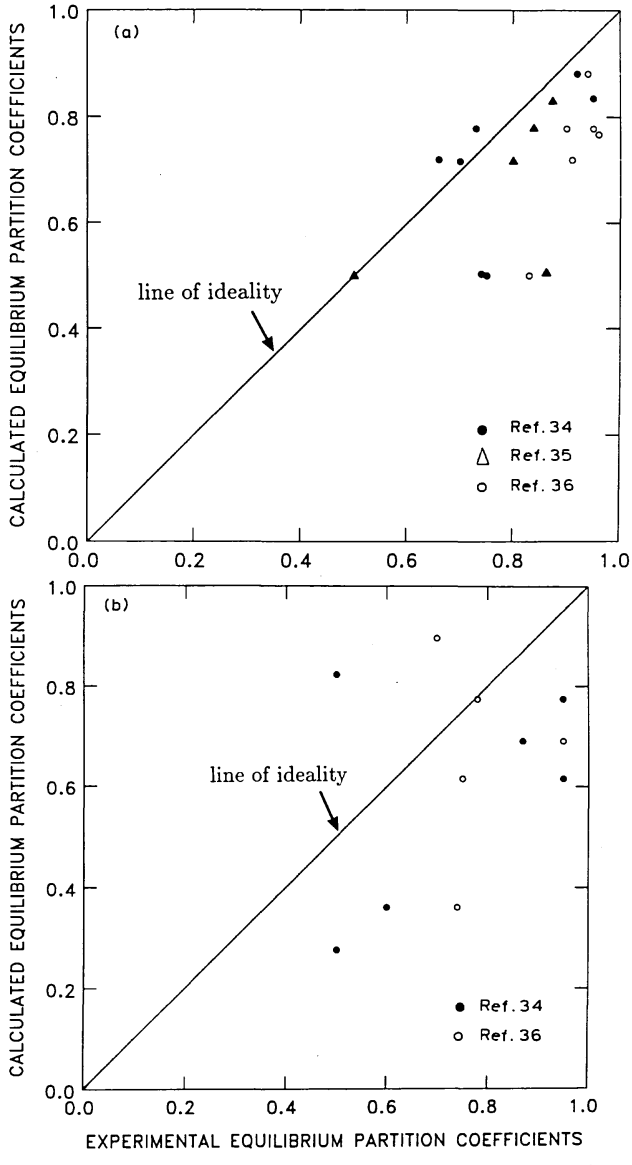

10 Calculated and experimental values for the equilibrium partition coefficients of solute elements for *a* δ-ferrite and liquid iron and *b* austenite and liquid iron

Summary

Standard free energy changes and activity data for iron and its binary and ternary alloys have been used to evaluate the general linear series (Wagner) expansion of the activity coefficient and these have themselves been used to generate an accurate thermodynamic determination of equilibrium multicomponent Fe–C–X transformation temperatures. A computer program has been written which accurately describes the influence of low concentrations of alloying elements on the Ae_3 equilibrium temperature of low alloy steels containing up to 1·8 wt-%C. Using the method of Kirkaldy and Baganis,[3] the phase boundary is calculated using empirical data to estimate the Gibbs free energy of the participating phases in the multicomponent system and the resultant deviation of the phase boundary from that of the binary Fe–C system is then found. New elements (V, Nb, W, Co) have been incorporated to the program and revised values for $\Delta^\circ G_0$, $\Delta^\circ H_0$, and T_o have been used. In addition, discrepancies with the Fe–Mn, Fe–Ni, and Fe–Nb systems have been resolved. The program has been shown to be valid for significant additions of Mn, Si, Ni, Cr, Mo, Cu, V, Nb, W, and Co.

The peritectic region of the phase diagram has been calculated, with each phase boundary being treated individually, and for the first time its accuracy evaluated. Results obtained by calculation have been compared with experimental data for the liquidi and solidi of a range of low alloy multicomponent steels and found to be in extremely good agreement. A good ability to predict the solidification

range, which strongly influences the amount of solute segregation, was also obtained. Finally, an attempt has been made to estimate the amount of partitioning for alloying elements between δ- and liquid iron, and between austenite and liquid iron, and agreement with observed results was fair. This model has been shown to predict accurately the modifications to the Fe–Fe_3C phase diagram of any given set of alloying elements, in the following range: (all wt-%) $C \leqslant 1{\cdot}8\%$, $Mn < 3{\cdot}0\%$, $Ni < 2{\cdot}5\%$, $Cr < 2{\cdot}5\%$, $Co < 2\%$, $Mo < 1{\cdot}5\%$, balance (including Si) $\leqslant 1{\cdot}0\%$. This covers the largest proportion of steels used in welding fabrication.

The practical limitations of the program result from two sources, i.e. the limitations of the theory itself, in particular the inability to account for solute–solute interactions, since it is only strictly correct for infinitely dilute solutions, and inadequate experimental data for the pure binary systems with iron as one component. It is anticipated that these source data will be refined as development of the program continues.

Acknowledgments

The authors are grateful to the Science and Engineering Research Council and to ESAB AB, Sweden, for financial support and to Professor D. Hull for the provision of laboratory facilities at the University of Cambridge. It is with pleasure that the authors acknowledge helpful discussions with members of the Phase Transformations Group at the University of Cambridge.

References

1. B. GRETOFT, H. K. D. H. BHADESHIA, and L.-E. SVENSSON: *Acta Stereol.*, 1986, **5**, (2), 365–371.
2. M. STRANGWOOD and H. K. D. H. BHADESHIA: in 'Welding metallurgy of structural steels', (Conf. Proc.), (ed. J. Y. Koo), 495–504; 1987, Warrendale, PA, The Metallurgical Society of AIME.
3. J. S. KIRKALDY and E. BAGANIS: *Metall. Trans.*, 1978, **9A**, (4), 495–501.
4. J. S. KIRKALDY, B. A. THOMSON, and E. A. BAGANIS: in 'Hardenability concepts with applications to steel', (Conf. Proc.), (ed. D. V. Doane and J. S. Kirkaldy), 82–125; 1978, Warrendale, PA, The Metallurgical Society of AIME.
5. L. S. DARKEN and R. W. GURRY: 'Physical chemistry of metals', 222–224; 1953, Tokyo, McGraw-Hill.
6. E. SCHÜRMANN, J. VON SCHWEINICHEN, R. VOLKER, and H. FISCHER: *Giessereiforschung*, 1987, **39**, (3), 97–103 and 104–113.
7. A. KAGAWA, K. IWATA, A. A. NOFAL, and T. OKAMOTO: *Mater. Sci. Technol.*, 1985, **1**, (9), 678–683.
8. P. CRASKA and R. B. McLELLAN: *Acta Metall.*, 1971, **19**, 1219–1225.
9. C. WAGNER: 'Thermodynamics of alloys', 51–52; 1952, London, Addison-Wesley.
10. H. K. D. H. BHADESHIA and D. V. EDMONDS: *Acta Metall.*, 1980, **28**, 1265–1273.
11. H. K. D. H. BHADESHIA: *Prog. Mater. Sci.*, 1985, **29**, 321–386.
12. H. HARVIG: *Jernkontorets Ann.*, 1978, **155**, 157–161.
13. L. KAUFMAN, E. V. CLOUGHERTY, and R. J. WEISS: *Acta Metall.*, 1963, **11**, (5), 323–335.
14. H. K. D. H. BHADESHIA: *Mater. Sci. Technol.*, 1985, **1**, (7), 497–504.
15. L. KAUFMAN and H. BERNSTEIN: in 'Refractory materials', Vol. 4, 19; 1970, New York, Academic Press.
16. M. COHEN: *Trans. AIME*, 1962, **224**, 638–656.
17. O. KUBASCHEWSKI: 'Iron-binary phase diagrams'; 1982, Berlin, Springer-Verlag.
18. J. B. GILMOUR, G. R. PURDY, and J. S. KIRKALDY: *Metall. Trans.*, 1972, **3**, 1455–1464.
19. R. C. HUDD, A. JONES, and M. N. KALE: *J. Iron Steel Inst.*, 1971, **209**, (2), 121–125.
20. K. W. ANDREWS: *J. Iron Steel Inst.*, 1956, **184**, 414–427.
21. M. HANSEN: 'The constitution of binary alloys', 676; 1958, New York, McGraw Hill.
22. H. I. AARONSON and H. A. DOMAIN: *Trans. AIME*, 1966, **236**, 781–796.
23. D. J. SWINDEN and J. H. WOODHEAD: *J. Iron Steel Inst.*, 1971, **209**, (11), 883–899.
24. R. A. GRANGE: *Met. Progr.*, 1961, **79**, (4), 73–75.
25. K. WATANABE: *Tetsu-to-Hagané (J. Iron Steel Inst. Jpn)*, 1975, **61**, 3069–3076.
26. R. C. COCHRANE: *Weld. World*, 1983, **21**, 16–24.
27. M. G. BENZ and J. F. ELLIOTT: *Trans. AIME*, 1961, **221**, 323–331.
28. T. B. MASSALSKI (ed.): 'Binary alloy phase diagrams', Vol. 1, 563; 1986, Metals Park, OH, ASM.
29. 'A guide to the solidification of steels', 155–156; 1977, Stockholm, Jernkontoret.
30. A. A. HOWE: *Ironmaking Steelmaking*, 1988, **15**, (3), 134–142.
31. H. FREDRIKSSON and L. HELLNER: *Scand. J. Metall.*, 1974, **3**, 61–68.
32. H. FREDRIKSSON: *Met. Sci.*, 1976, **10**, (3), 77–86.
33. T. EDVARDSSON, H. FREDRIKSSON, and I. SVENSSON: *Met. Sci.*, 1976, **10**, (9), 298–306.
34. Z. MORITA and T. TANAKA: *Trans. Iron Steel Inst. Jpn*, 1983, **23**, (10), 824–833.
35. Z. MORITA and T. TANAKA: *Trans. Iron Steel Inst. Jpn*, 1984, **24**, (3), 206–211.
36. A. KAGAWA and T. OKAMOTO: *Mater. Sci. Technol.*, 1986, **2**, (10), 997–1008.